Kämpf, L., Müller, P., Höllerer, H., Plessen, B., Naumann, R., Thoss, H., Güntner, A., Merz, B., Brauer, A. (2015): Hydrological and sedimentological processes of flood layer formation in Lake Mondsee. - *The Depositional Record*, *1*, 1, p. 18-37.

DOI: http://doi.org/10.1002/dep2.2

The Depositional Record
The journal of the International Association of Seidmentologisits
Open Access

ORIGINAL RESEARCH ARTICLE

Hydrological and sedimentological processes of flood layer formation in Lake Mondsee

LUCAS KÄMPF*,†, PHILIP MUELLER‡, HANNES HÖLLERER§, BIRGIT PLESSEN*, RUDOLF NAUMANN¶, HEIKO THOSS‡, ANDREAS GÜNTNER‡, BRUNO MERZ‡ and ACHIM BRAUER*

*Section 5.2 Climate Dynamics and Landscape Evolution, GFZ German Research Centre for Geosciences, Telegrafenberg, Potsdam, 14473, Germany
†TU Dresden, Faculty of Environmental Sciences, Institute for Soil Science and Site Ecology, Pienner Strasse 19, Tharandt, 01737, Germany
‡Section 5.4 Hydrology, GFZ German Research Centre for Geosciences, Telegrafenberg, Potsdam, 14473, Germany
§Research Institute for Limnology Mondsee, University of Innsbruck, Mondseestrasse 9, Mondsee, 5310, Austria
¶Section 4.2 Inorganic and Isotope Geochemistry, GFZ German Research Centre for Geosciences, Telegrafenberg, Potsdam, 14473, Germany

Keywords
Detrital layers, flood reconstruction, flood-related sediment flux, Lake sediments, monitoring, process understanding.

Manuscript received: 19 December 2014; Accepted: 14 May 2015

The Depositional Record **2015, 1(1):18–37**

doi: 10.1002/dep2.2

ABSTRACT

Detrital layers in lake sediments are recorders of extreme flood events. However, their use for establishing time series of past floods is limited by lack in understanding processes of detrital layer formation. Therefore, we monitored hydro-sedimentary dynamics in Lake Mondsee (Upper Austria) and its main tributary, Griesler Ache, over a 3-year period from January 2011 to December 2013. Precipitation, discharge and turbidity were recorded continuously at the river outlet to the lake and compared to sediment fluxes trapped with 3 to 12 days resolution at two locations in the lake basin, in a distance of 0·9 (proximal) and 2·8 km (distal) to the Griesler Ache inflow. Within the 3-year observation period, 26 river floods of different magnitude (10 to 110 $m^3\ s^{-1}$) have been recorded resulting in variable sediment fluxes to the lake (4 to 760 $g\ m^{-2}\ d^{-1}$) including the 'century-scale' flood event in June 2013. The comparison of hydrological and sedimentological data revealed (i) a rapid sedimentation within 3 days after the peak runoff in the proximal and within 6 to 10 days in the distal lake basin; (ii) empirical flood thresholds for triggering sediment flux at the lake floor increasing from the proximal (20 $m^3\ s^{-1}$) to the distal lake basin (30 $m^3\ s^{-1}$) and (iii) various factors that control the detrital sediment transport in the lake. The amount of sediment transported to the lake is controlled by runoff and catchment sediment availability. The distribution of detrital sediment within the lake basin is mainly driven by mesopycnal interflows and closely linked to flood duration and the season in which a flood occurred. The combined hydro-sedimentary monitoring revealed detailed insights into processes of flood layer formation in a meso-scale peri-Alpine lake and, thereby, improves the interpretation of the depositional record of flood layers.

INTRODUCTION

Lakes form ideal sediment traps in the landscape continuously recording land surface processes in the catchment including extreme events (Hsü & Kelts, 1985). Discrete flood-triggered sediment fluxes of detrital catchment material into lakes result in the formation of discrete detrital layers at the lake floor (Sturm & Matter, 1978; Siegenthaler & Sturm, 1991). Therefore, detrital layers in lake sediments are increasingly used to establish long flood chronologies especially in the Alpine (Støren *et al.*, 2010; Glur *et al.*, 2013; Wilhelm *et al.*, 2013; Wirth *et al.*, 2013b), peri-Alpine (Arnaud *et al.*, 2005; Czymzik *et al.*, 2013; Swierczynski *et al.*, 2013) and Arctic realms (Francus *et al.*, 2002; Lamoureux *et al.*, 2006; Lapointe *et al.*, 2012). The recurrence intervals of detrital layers provide

information about palaeoflood frequencies (Czymzik *et al.*, 2010; Swierczynski *et al.*, 2012; Schlolaut *et al.*, 2014), whereas flood intensities have been inferred from the thickness (Schiefer *et al.*, 2011; Wilhelm *et al.*, 2013) of individual deposits.

Varved sediment records provide, in addition, the unique opportunity to date detrital layers with seasonal precision (Mangili *et al.*, 2005) and, thereby, (i) determine palaeoflood variability even at seasonal scale (Swierczynski *et al.*, 2012; Wirth *et al.*, 2013a) and (ii) calibrate the sub-recent detrital layer record with instrumental flood data (Francus *et al.*, 2002; Chutko & Lamoureux, 2008; Czymzik *et al.*, 2010).

Commonly, flood reconstruction from lake sediments assume the completeness of the depositional record in the sense that each flood resulted in a well-preserved detrital layer. However, a test of the hypothesis of completeness of the depositional record is still lacking. First detailed comparisons of detrital layer records with instrumental data even questioned the assumption of completeness by providing evidence for both, floods that did not result in detrital layer deposition and detrital layers, which were not triggered by strong floods (Czymzik *et al.*, 2010; Kämpf *et al.*, 2012b). A possible reason might be that the amount and spatial distribution of detrital sediment within a lake basin triggered by flood events might vary (Lamoureux, 1999; Jenny *et al.*, 2014) probably even depending on the season in which a flood occurred (Kämpf *et al.*, 2014). A better knowledge of the hydrological and sedimentary processes of detrital layer formation is required to reduce the bias in interpretation and, thereby, improve the use of depositional records as palaeoflood archives.

To gain a more sophisticated process understanding of detrital layer formation different attempts have been initiated comprising detailed analyses of single flood deposits (Gilbert *et al.*, 2006; Kämpf *et al.*, 2012a) and *in situ* monitoring of flood triggered sediment fluxes (Best *et al.*, 2005; Crookshanks & Gilbert, 2008; Dugan *et al.*, 2009). Most observational studies of detrital sediment fluxes in lakes have been performed in arctic and high mountain lakes with predominantly clastic sedimentation. Despite of the growing number of flood reconstructions from Alpine and peri-Alpine lakes (e.g. Wirth *et al.*, 2013b), in-depth monitoring studies in such lakes with mainly autochthonous sediments (biochemically precipitated calcite and organic components) are still lacking.

Here, we present results of a 3-year integrated lake and catchment monitoring of flood and sediment dynamics in the peri-Alpine Lake Mondsee. The study period comprises the 'century-scale' flood event in June 2013 (Blöschl *et al.*, 2013). We chose Lake Mondsee for this in-depth monitoring since it provides a varved sediment record and a flood layer record covering the last 7100 years (Swierczynski *et al.*, 2013) as well as a good data base of meteorological and hydrological data. In addition, a first calibration of sub-recent detrital layers with instrumental flood data is available (Kämpf *et al.*, 2014). Ultimately, we will contribute new knowledge about flood layer formation in a meso-scale peri-Alpine lake, which is expected to generally improve flood reconstructions from depositional records of lakes.

STUDY SITE

Lake Mondsee is located at the northern fringe of the European Alps in Upper Austria (47°48′N, 13°23′E) at an altitude of 481 m above sea-level (a.s.l.) (Fig. 1). With a surface area of 14 km^2 and a maximum water depth of 68 m Lake Mondsee is a meso-scale peri-Alpine lake characterized by a specific morphometry displaying a significant kink in the generally elongated and NW-SE directed shape (Fig. 1). Lake Mondsee is a meromictic hardwater lake (Dokulil & Skolaut, 1986) with one mixing period in autumn/winter and thermal stratification between May and September (Fig. 2). Episodically, the lake is completely ice-covered which happened once during the observation period in February to March 2012.

The catchment (247 km^2) is subdivided into two major geological units by a main Alpine thrust fault (Van Husen, 1989) following the southern shoreline of the lake (Fig. 1). The northern catchment (ca. 75% of the total catchment) is formed by peri-Alpine hills of up to 1100 m a.s.l. which are built up by Cretaceous Flysch sediments (Sandstone, Argillite). The valleys are covered by moraines formed by latest Pleistocene glacier activity (Van Husen, 1989). Three tributaries drain the northern catchment: the Griesler Ache in the West, the Zeller Ache in the North and the Wangauer Ache in the East. Regarding its size and runoff variability (A_0 = 110 km^2; MQ = 4 $m^3\ s^{-1}$; HHQ = 137 $m^3\ s^{-1}$, ref. BMLFUW (2011)), the Griesler Ache is the largest tributary to Lake Mondsee and the main source for suspended sediments during floods (Kämpf *et al.*, 2014). The southern sub-catchment (ca. 25%) reaches a maximum elevation of 1700 m a.s.l. and is part of the Northern Calcareous Alps. The base rock is composed of Jurassic and Triassic units of limestone and dolomite forming steep slopes at the southern lake shoreline which are drained by small torrents like, for example, the Kienbach creek with a catchment of 2·1 km^2 (Fig. 1). Lake Mondsee drains via the river Seeache into Lake Attersee at the south-eastern end of the lake (Fig. 1).

METHODS

A monitoring network was installed in Lake Mondsee and its catchment between 2011 and 2012, comprising

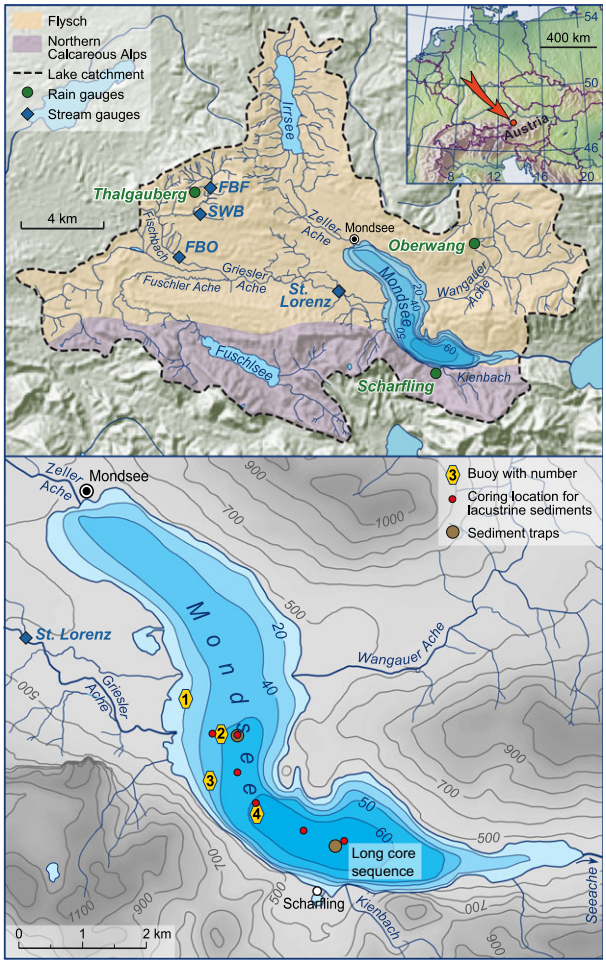

Fig. 1. Lake Mondsee catchment and monitoring set-up including (i) four stream gauges equipped with devices for measuring precipitation, water level, air and water temperature, electrical conductivity, turbidity and automated water sampling, (ii) four monitoring buoys within the lake for multilevel water current and turbidity monitoring (Mueller *et al.*, 2013) and (iii) two sediment trap chains equipped with three integral traps in different water depths, one sequential trap at the lake floor and thermistors in different water depths. Additional rain gauges in the catchment conducted by the hydrographic services of Upper Austria and Salzburg are also indicated. Six surface sediment cores were recovered along a transect from the Griesler Ache inflow towards a long sediment core in the distal lake basin (Swierczynski *et al.*, 2013).

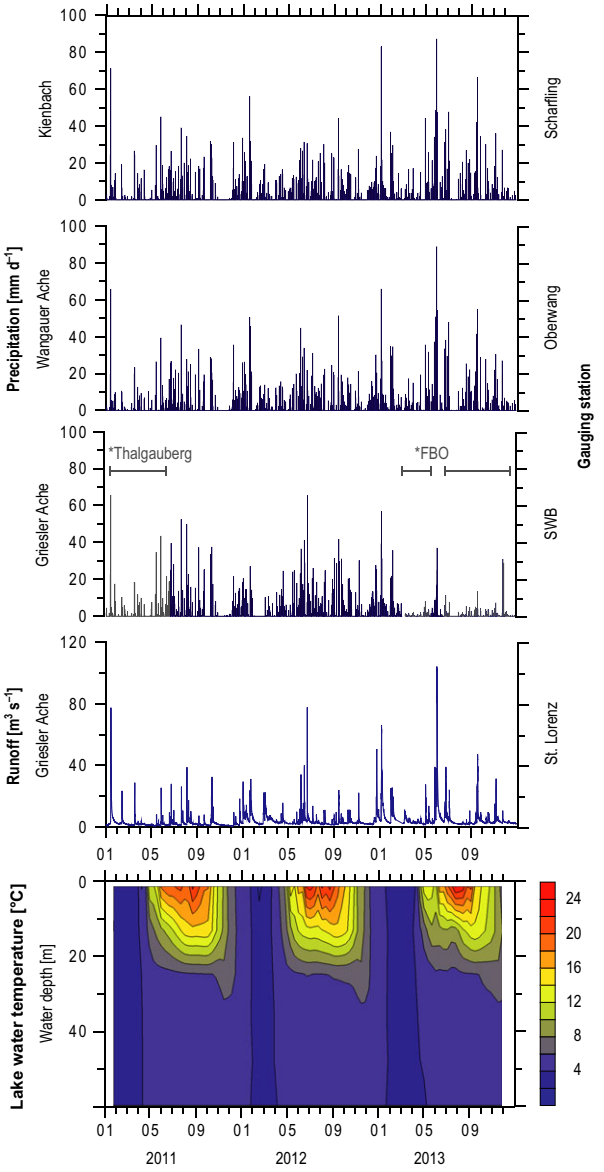

Fig. 2. Hydroclimatic data 2011 to 2013: daily precipitation sums from different catchments: Kienbach (Scharfling rain gauge), Wangauer Ache (Oberwang), and Griesler Ache [Streuwiesenbach (SWB), gaps in the time series were filled with data from Thalgauberg and Fischbach Outlet (FBO) rain gauges]; hourly runoff of the Griesler Ache River at St. Lorenz gauging station and water column temperature at the proximal trap site. Locations of the gauging stations can be found in Fig. 1.

four river gauges along the main tributary to Lake Mondsee, the Griesler Ache, as well as four monitoring buoys and two sediment trap chains within the lake (Fig. 1). The combination of river gauges and monitoring buoys was designed to track hydro-sedimentary dynamics, i.e. runoff generation and sediment transport, continuously from the head catchments to the lake (Mueller *et al.*, 2013).

Catchment monitoring

Precipitation in the Griesler Ache catchment is recorded since June 2011 using OTT Pluvio rain gauges (OTT Hydromet, http://www.ott.com) at the gauging stations St. Lorenz located close to Lake Mondsee (482 m a.s.l., 4 km distance to inflow), Fischbach Outlet (FBO, 552 m,

10 km) located at the confluence of the Griesler Ache and the Fischbach, which is the largest tributary to the Griesler Ache, and at two stations in the Fischbach head-catchment, Streuwiesenbach (SWB, 777 m, 11 km) and Fischbach Forest (FBF, 786 m, 12 km). In addition we used data from three precipitation gauges at Thalgauberg in the Griesler Ache catchment (730 m a.s.l., 11 km distance to inflow) (operated by the Hydrographic Survey of Salzburg), Scharfling in the Kienbach catchment (482 m, 0·7 km) and Oberwang in the Wangauer Ache catchment (595 m, 5 km) (both operated by the Hydrographic Survey of Upper Austria). Runoff data were obtained from the stream gauge of St. Lorenz (Hydrographic Survey of Upper Austria), located 4 km upstream of the Griesler Ache inflow to Lake Mondsee (Fig. 1). For monitoring sediment transport in the river, the station was additionally equipped with a FTS DTS-12 turbidity sensor (Forest Technology Systems Inc., http://www.ftsenvironmental.com) and an ISCO 3700 automatic pumping sampler (Teledyne ISCO, http://www.isco.com). Depending on the actual values of discharge and turbidity, 3 to 24 river water samples (1 l) were taken automatically for each of 21 flood events since June 2011 following the turbidity-threshold-sampling (Lewis, 1996).

Lake monitoring

Two moorings were installed in Lake Mondsee, each equipped with one sequencing sediment trap (S-trap) and three integrating sediment traps (I-traps). The locations follow a transect from the inflow of the Griesler Ache river to the location of a long sediment record used for establishing a flood layer chronology over the last 7100 years (Swierczynski *et al.*, 2013), with one mooring in a distance of 900 m to the river mouth (proximal trap: 47°49·21′N, 13°22·78′E, water depth: 56 m) and the other in a distance of 2800 m (distal trap: 47°48·32′N, 13°23·92′E, water depth: 63 m). We compared the sediment trap data with detrital layers investigated in surface sediment cores that were previously retrieved close to the trap locations in the proximal (sediment core MO/10/4: 47°49·16′N, 13°22·79′E) and distal lake basin (MO/05/P3: 47°48·41′N, 13°24·09′E, ref. Kämpf *et al.* (2014)).

The I-traps (UWITEC, http://www.uwitec.at) have two collecting cylinders with an active area of 127 cm^2 in total. The two sequencing traps are equipped with a computer programmable sample bottle carrousel and differ in size: with 500 cm^2 we chose a trap with a smaller active for the proximal location (PPS 4/3, 12 sample bottles, Technicap, http://www.technicap.com) and a larger one for the distal location (1250 cm^2, PPS 3/3, 12 sample bottles) due to expected higher sediment accumulation ratios closer to the inflow of the Griesler Ache (Swierczynski *et al.*, 2009). The S- and one of the I-traps were deployed approximately 3 m above the lake bed surface in a water depth of 53 m (prox.) and 60 m (dist.). The other two I-traps were moored in the upper water column (14 m) and between the upper and lower traps (prox.: 33 m, dist.: 30 m). 12 temperature loggers (Hobo U22 Water Temp Pro, Hobo, http://www.onsetcomp.com) were attached to the proximal mooring at water depths of 1, 3, 5, 8, 11, 14, 18, 22, 33, 43, 53 and 55 m and 4 loggers to the distal mooring at water depths of 1, 14, 30 and 60 m.

The moorings were first deployed at 13 January 2011. The S-trap at the distal mooring was added on 04 April 2012. The traps were recovered in a monthly rhythm between April and November until 03 April 2014. Thus, I-traps collect material on a basis of 21 to 41 days between April and November and of 41 to 123 days between December and March. The individual S-trap samples cover a time interval of 3 to 4 days between April and November and 4 to 12 days between December and March.

This study reports data from samples collected between January 2011 and December 2013 giving a total of 28 I-trap samples from the upper (14 m) and lower (prox.: 53 m, dist.: 60 m) water column at each location as well as 269 S-trap samples at the proximal and 158 samples at the distal location. The S-trap time series exhibit three gaps: (i) between March and April 2012 (37 days) caused by persistent ice cover, (ii) between September and October 2012 (21 days) due to technical reasons and (iii) in June 2013 (6 days) due to very high lake water level that inhibited trap recovery. The third gap was bridged by deploying two additional I-traps close to the mooring locations.

Sediment analyses

The sample bottles of the river water samplers and sediment traps were stored at 4°C after recovery for at least 48 h to ensure that all suspended particles had settled. The samples were freeze dried and the total dry weight was determined. For trap samples, the daily sediment flux (in g m^{-2} d^{-1}) was calculated for each sample. For river water samples, the measured suspended sediment concentration (SSC in g L^{-1}) was used for setting up SSC rating curves of the turbidity sensor at the gauge of St. Lorenz (Figure S2). The rating curves were established individually for the three strongest recorded floods by applying polynomial regression (Lewis & Eads, 2009).

Total carbon (TC), nitrogen (TN) and organic carbon (TOC) were determined for each S-trap sample using an elemental analyser Euro Vector EA (EuroEA 3000, www.eurovector.it). For TC and TN, around 5 mg of powdered sample was loaded in tin capsules and

combusted in the elemental analyser. TOC was determined on *in situ* decalcified samples. Around 3 mg of sample was weighted into Ag-capsules, treated with 20% HCl, heated for 3 h at 75°C, and finally wrapped and measured as described above. Replicate determinations showed a standard deviation better than 0·2%. Organic matter (OM) was calculated as OM = 2 × TOC (Meyers & Teranes, 2001) and total inorganic carbon (TIC) as TIC = TC-TOC. The $CaCO_3$ content was calculated stoichiometrically by multiplying the TIC by 8·33, assuming that all inorganic carbon is bound as calcium carbonate. We are aware that minor dolomite contributions from catchment rocks (Figure S1) in the detrital carbonate fraction might cause little inaccuracies.

Grain size was measured for 13 selected trap samples with high sediment flux rates using a laser particle sizer (Fritsch Analysette, Fritsch, http://www.fritsch.de). The samples were sieved at 1 mm and dispersed in an ultrasonic bath before measuring. Image data were automatically transferred to particle distribution by the software Fritsch MaScontrol applying the Fraunhofer model.

The mineralogical composition was determined for those trap samples that were also analysed for their grain size distribution and for four samples of river bed material as well as two detrital layers in sediment cores using a PANanlytical Empyrean X-ray diffractometer equipped with a Cu tube (http://www.panalytical.com). The samples were powdered before measuring.

RESULTS

Hydro-climatic conditions at Lake Mondsee 2011 to 2013

Mean annual precipitation in the Mondsee catchment during the observation period from January 2011 to December 2013 was 1600 mm and thus, in the range of the long-term mean (1981 to 2011, ref. BMLFUW (2011)). Large rainfall amounts (>40 mm d^{-1}) were recorded during 20 days (2011; 4, 2012: 7, 2013: 9) and primarily took place between May and September (15 days) and, secondarily, in winter (5 days >40 mm). With 90 mm d^{-1} the maximum precipitation was recorded at the Oberwang rain gauge on 01 June 2013 (Fig. 2).

The mean runoff between January 2011 and December 2013 was 4·1 m^3 s^{-1} that is close to the long-term mean of 3·9 m^3 s^{-1} (1961 to 2011, ref. BMLFUW (2011)). Runoff events >30 m^3 s^{-1} occurred 14 times in the observation period (2011: 3, 2012: 4, 2013: 7) and, like precipitation events, cumulated in summer (May-Sep: 8, Oct-Nov: 2, Dec-Feb: 4). The largest flood in the monitoring period reached a maximum hourly discharge of 104 m^3 s^{-1} (2 June 2013) and was one of the strongest recorded floods in that region with an estimated return period of around 100 years (Eybl *et al.*, 2013).

Variability in sediment flux I: total sediment composition

Sediment flux in Lake Mondsee was trapped over the period from January 2011 to December 2013 at two different sites within the lake basin (Fig. 1), one located in a position proximal to the inflow of the main tributary river (distance: 900 m) and one in a distal position (2800 m). The total sediment flux including both, lake internal (autochthonous) and external (allochthonous) components, was by median 4 g m^{-2} d^{-1} (prox.: 4·2 g m^{-2} d^{-1}, dist.: 3·6 g m^{-2} d^{-1}) and exhibited (i) a seasonal variability with higher mean flux rates in summer (5 to 6 g m^{-2} d^{-1} in May-Sep) and lower mean flux rates in autumn and winter (1 to 1·5 g m^{-2} d^{-1} in Oct-Jan) and (ii) short-term peaks of up to 758 g m^{-2} d^{-1} in the proximal and up to 59 g m^{-2} d^{-1} in the distal lake basin (Fig. 3A and B).

The seasonal variability of the trapped sediment flux is also expressed by distinct changes in sediment composition (Fig. 3C and D). Calcite contents varied from 20 to 40% (October to April) to 60 to 95% (May to September) with maximum values between July and August (Fig. 3C). The higher calcite contents in summer reflect biochemical precipitation of calcite in epilimnic waters which is a typical seasonal process in mid-latitude hardwater lakes (Koschel *et al.*, 1983). The contents of organic matter in trapped sediment, calculated from the measured TOC contents, varied between 5 and 25% and exhibited a clear maximum in April and a second, lower maximum of 15 to 20% in late autumn (October-December) when bulk sediment fluxes were lowest (Fig. 3B and D). The maximum in April was predominantly made up of diatom frustules, whereas in autumn amorphous organic matter and diatoms were abundant as revealed by smear slide investigations. Between October and March and within peak sediment flux samples the sediment was mainly composed of dolomitic and siliciclastic matter. The observed seasonal variations in sediment flux lead to the formation of characteristic diatom, calcite and mixed sub-layers preserved and described in the varved sediment record of Lake Mondsee (Lauterbach *et al.*, 2011; Swierczynski *et al.*, 2012).

Variability in sediment flux II: spatial distribution

We characterized the spatial sediment distribution in the lake water body by both its vertical and horizontal

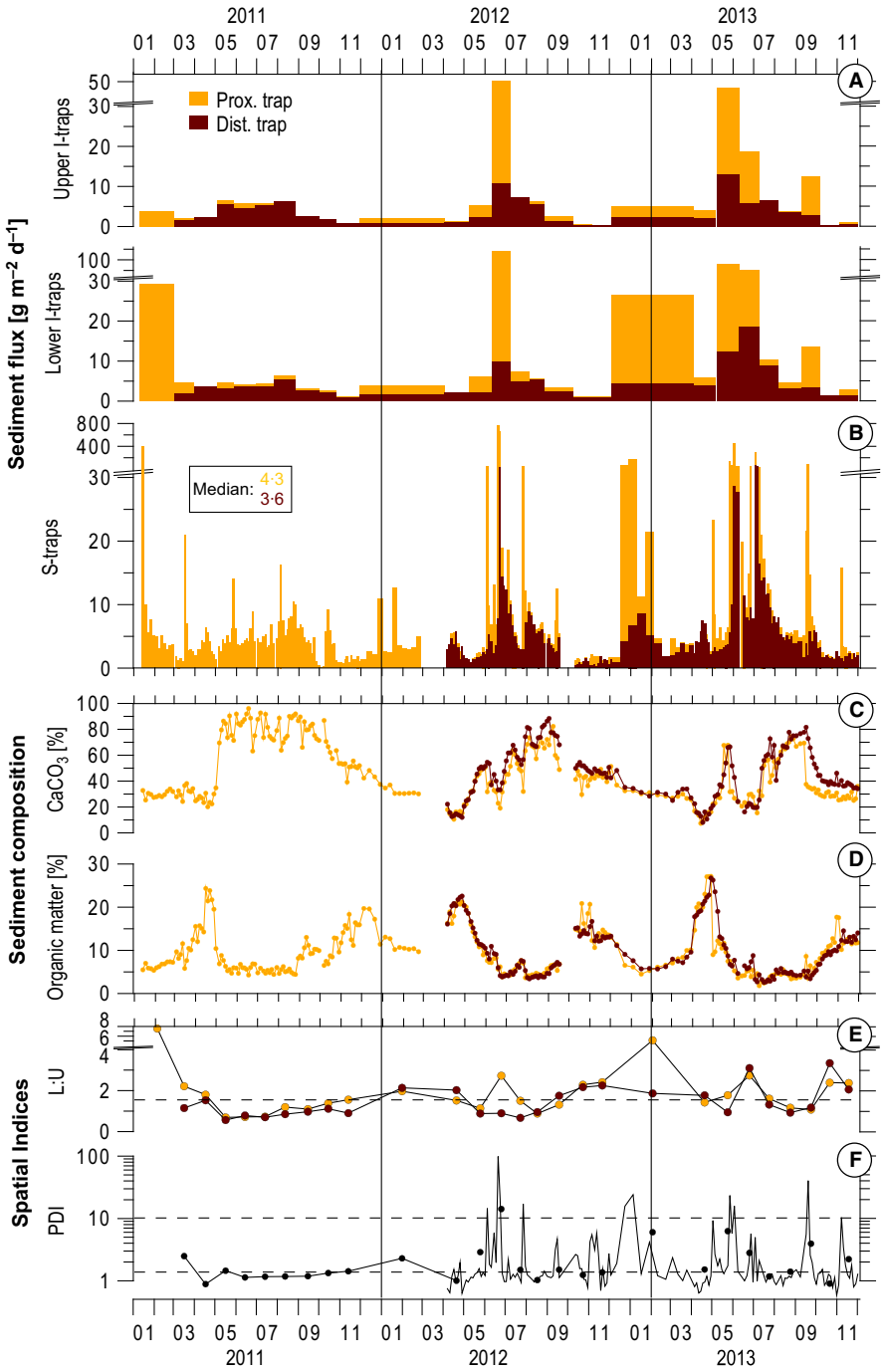

Fig. 3. Sediment fluxes in Lake Mondsee at the proximal and distal location (01/2011 to 11/2013): (A) monthly values in integrating traps in the upper (14 m water depth) and lower water column (3 m above lake floor, prox.: 53 m, dist.: 60 m); (B) 3 to 12 days values in sequential traps in the lower water column and contents of (C) calcite and (D) organic matter (Prox.: 2011 to 2013, dist.: 2012 to 2013). Spatial sediment flux patterns are expressed by ratios of sediment flux between: (E) lower and upper traps (L : U) and (F) proximal and distal traps (PDI), dots in (F) indicate monthly values calculated from I-traps.

variability in order to decipher pathways and mechanisms of lake internal sediment transport. The vertical variability is expressed by the flux ratio of the lower and upper traps (L : U, ref. Cockburn & Lamoureux (2008)) calculated for the 28 I-trap samples representing monthly means (Fig. 3E). From these samples, 51% (prox.: 13 samples,

dist.: 16 samples) ranged between 0·6 and 1·5 indicating comparable flux rates throughout the water column and 38% of the values ranged between 1·5 and 2·5 (prox.: 12 samples, dist.: 9 samples) representing a mixture of vertical and lateral sediment fluxes. L : U values >2·5 rarely occurred (11%, prox.: 4 samples, dist.: 2 samples), reflecting sediment flux predominately in the lower water column mainly driven by hyperpycnal underflows (Cockburn & Lamoureux, 2008). It has to be considered that the vertical sediment flux ratios likely represent minimum estimates of sedimentation during times of underflows, as the traps were designed to capture mainly sediment that settled vertically through the water column and were allocated 3 m above the lake bottom likely leading to an underestimation of material transported by underflows. The vertical sediment distribution indicates seasonally changing sediment pathways. In summer (May-Sep), the L : U ratio was <1·5 for 90% of all values indicating predominately downward sediment flux from the upper water column. In fall to spring the L : U ratio was >1·5 for 90% of all values pointing to the contribution of lateral sediment transport from the shoreline and/or the tributary streams during winter.

The lateral sediment distribution is expressed by the flux ratio of the proximal and the distal site (Proximal-Distal Index [PDI], ref. Lamoureux (1999)). PDI values were calculated for the lowermost I-traps and sequential traps (Fig. 3F) revealing 64% of the values ranging between 0·6 and 1·5 representing a uniform sedimentation pattern and 36% of the values at the proximal site exceeding those at the distal site by factors >1·5 proving sediment input from the main tributary river and decreasing sediment deposition towards distal direction through settling of particles. In few cases (6%) the PDI values exceed 10 indicating localized sediment fluxes to the proximal lake basin.

To identify events with strongly increased sedimentation in the sediment flux time series, we defined high sediment flux values as peaks which (i) exceeded the median sediment flux of 4 g m^{-2} d^{-1} and (ii) showed an increase to the previous sample of more than 50%. This resulted in 32 sediment flux peaks occurring during 35 months of observation at the proximal trap location (2011 to 2013) and 14 peaks during 20 months of observation at the distal trap location (2012 to 2013) (Fig. 4). 12 of these 14 peaks occurred synchronously at both locations or

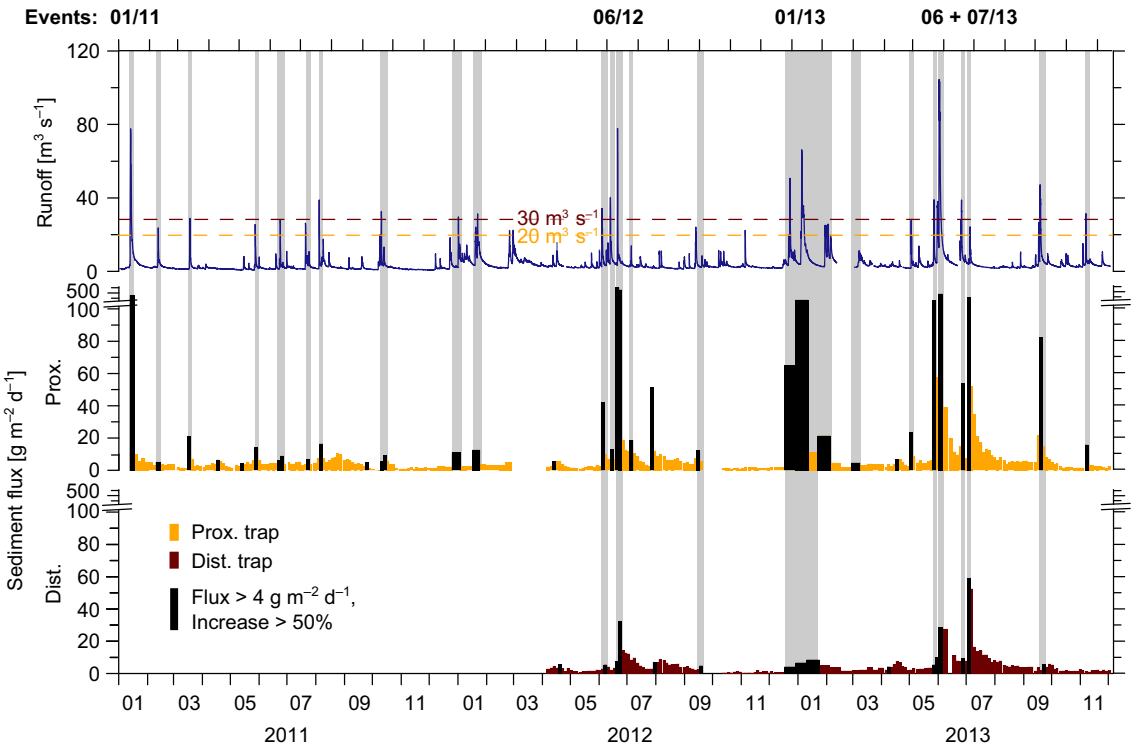

Fig. 4. Comparison of trapped sediment flux in Lake Mondsee with runoff in the Griesler Ache River. Black coloured samples mark peaks in sediment flux as defined by exceeding the median sediment flux (4 g m^{-2} d^{-1}) and an increase to the previous sample of 50%. Grey bars mark sediment flux peaks coincided with elevated runoff. Dashed lines indicate thresholds for triggering peaks in sediment flux: 20 m^3 s^{-1} in the proximal and 30 m^3 s^{-1} in the distal lake basin. The five runoff events that triggered the highest sediment flux to the lake basin (>100 g m^{-2} d^{-1} at the proximal trap) are named at the top.

delayed by one sample at the distal location. Four peaks occurred only in one part of the basin; two at the proximal and two at the distal trap. For peak sediment flux events at both trap sites the spatial distribution of detrital material is variable expressed in PDI values ranging between 2 and 25.

Sediment flux versus runoff

The 3-year time series of trapped sediment flux was compared to runoff data from the outlet gauge of the main tributary river, the Griesler Ache, in order to test if a relation exists between river floods and the spatio-temporal sediment distribution within the lake (Fig. 4). Most of the defined peaks in sediment flux (prox.: 26 of 32; flux: 5 to 758 g m^{-2} d^{-1}; dist.: 11 of 14; 4 to 59 g m^{-2} d^{-1}) coincided with elevated river runoff ranging from 10 to 104 m^3 s^{-1}. For one peak in sediment flux (July 2012), no discharge data were available so that this event was excluded from further analyses. Five peaks of the proximal (16% of all sediment flux peaks) and two peaks of the distal trap (15%) did not relate to elevated runoff. Interestingly, peaks not related to runoff events occurred independently either at the proximal or at the distal site (Fig. 4).

Comparing flood magnitudes in terms of their hourly peak river discharge reveals that 10% of low magnitude floods in the range 10 to 20 m^3 s^{-1} triggered a measurable peak in sediment flux in the proximal lake basin, whereas for floods >20 m^3 s^{-1} already 96% resulted in a distinct sediment flux at this location (Fig. 4). At the distal location elevated sediment flux was never observed for floods <20 m^3 s^{-1}, but 80% of floods >30 m^3 s^{-1} resulted in a peak. Two peaks in sediment flux at the distal location were related to floods between 20 and 30 m^3 s^{-1}. The sediment flux peaks in the proximal lake basin occurred within 3 days after the discharge peak, i.e. within the same sampling interval (Fig. 5). In the distal lake basin the period of highest sediment flux mostly expanded over two sampling intervals (3 to 6 days).

Besides the coincidence of flood occurrence and enhanced sediment flux, we compared the amount of sediment deposited over the whole flooding period with peak runoff values and observed an exponential relation (Fig. 6A). The correlation coefficient decreases from the proximal ($r^2_{prox.}$ = 0·62) to the distal lake basin ($r^2_{dist.}$ = 0·31) and is strongly affected by one event (07/13, Fig. 4), when a very high sediment deposition (prox.: 1258 g m^{-2}, dist: 468 g m^{-2}) but only a low maximum discharge were recorded (24 m^3 s^{-1}). If this event is

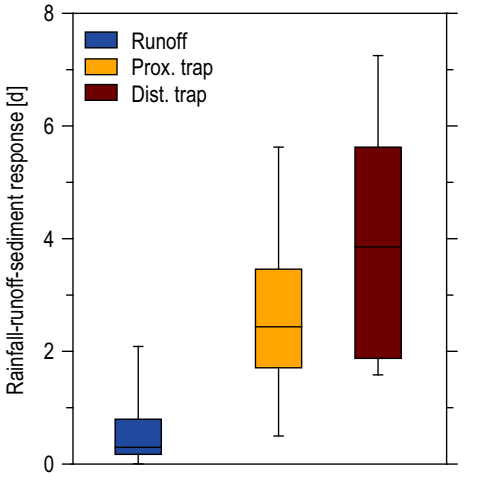

Fig. 5. Time lag between peaks in precipitation and runoff as well as between peaks in runoff and sediment flux at the proximal and distal traps (end of sampling interval) of (prox.: *n* = 25, dist.: *n* = 7).

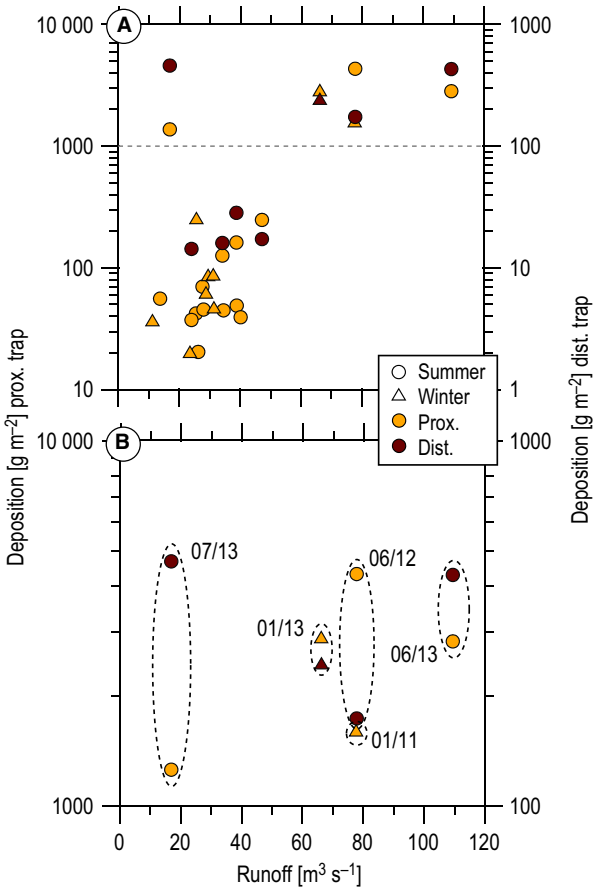

Fig. 6. (A) Correlation of peak runoff (hourly values) and sediment deposition during the monitoring period 2011 to 2013 applying an exponential regression. Statistics: Prox.: *n* = 25, r^2 = 0·76, *P* < 0·01, Dist.: *n* = 7, r^2 = 0·80, *P* < 0·01; 07/13 event excluded from statistics. (B) Enlarged view of plot (A) for the five strongest sediment flux events.

excluded, the correlation becomes better and more similar at both sites ($r^2_{prox.}$ = 0·76, $r^2_{dist.}$ = 0·80).

Hydro-sedimentary dynamics during major floods

In total, 26 floods resulting in enhanced sediment flux to the lake floor were recorded in the 3-year monitoring period. For five of these floods the sediment yield exceeded 1000 g m^{-2} at the proximal site (1258 to 4320 g m^{-2}) that were triggered by precipitation of more than 40 mm d^{-1} and resulting runoff peaks ranging from 24 to 104 m^3 s^{-1} (Table 1). At the distal site the sediment yield was significantly lower (174 to 468 g m^{-2}).

Three of the five floods with highest sediment yields occurred in summer and two in winter (Table 1). The 01/11 flood lasted for 3 days with a maximum precipitation of more than 65 mm d^{-1} in all three gauged catchments (Fig. 2). The 01/13 event was characterized by a persistent wet phase over 2 months with two main precipitation periods of 3 and 4 days, respectively, and maxima of 57 to 83 mm d^{-1} (Fig. 8). Whereas the two winter floods were both triggered by precipitation events that covered the whole catchment area, the three strongest summer floods were triggered by regional and local scale rainfall events (Fig. 2). The latter were convective events of high intensity and short duration (<1 day) affecting only parts of the catchment, like the 06/12 event in the Fischbach sub-catchment (max. rainfall at station SWB: 65 mm d^{-1}) and the 07/13 event in the Wangauer Ache catchment (Oberwang: 48 mm d^{-1}). In contrast, the 06/13 event was triggered by a series of synoptic scale low pressure systems (Blöschl *et al.*, 2013), resulting in strong precipitation over the whole catchment area lasting for 2 weeks (Table 1).

The stream-flow rose within 1 to 10 h after the main precipitation events (Figs 7 and 8). In January 2011, the flood hydrograph peaked at 78 m^3 s^{-1} and was larger than 10 m^3 s^{-1} for 3 days. The two runoff peaks between December 2012 and January 2013 were characterized by maximum discharges of 50 and 66 m^3 s^{-1} and durations of 3 and 7 days. The local rainfall events in June 2012 and July 2013 triggered peak flows of 78 m^3 s^{-1} during the 06/12 event and 24 m^3 s^{-1} during the 07/13 event. The comparably low peak flow in the Griesler Ache during the 07/13 event is due to the local character of the precipitation event which mainly covered the catchment of the Wangauer Ache which is not part of our

Table 1. Hydro-sedimentary data on the five largest sediment transfer events to Lake Mondsee within the monitoring period 2011 to 2013. Note that the 07/13 event is a very rare local event transporting sediments from a different sub-catchment (Wangauer Ache) that is not included in the monitoring program.

	01/11	06/12	01/13	06/13	07/13
Catchment data					
Precipitation					
Affected catchment area	Regional	Fischbach	Regional	Regional	Wangauer A.
Date	10 to 15 Jan	20 Jun	9 Dec to 12 Jan	19 May to 06 Jun	03 to 05 Jul
Days >10 mm	2	1	3+3+4	1+2+4	2
Maximum [mm d^{-1}]	71	65	83	90	48
Sum [mm]	104	82	350	320	75
Discharge Griesler Ache					
Days >10 m^3 s^{-1}	3	1	3+7	1+8	1
Max. hourly discharge [m^3 s^{-1}]	78	78	66	104	24
Max. daily discharge [m^3 s^{-1}]	56	21	43	79	11
Max. turbidity [NTU]	No data	1730	1078	1410	No data
Max. measured SSC [g L^{-1}]	No data	19	1	62	No data
Max. rated SSC [g L^{-1}]	No data	20	2	103	No data
Lake data					
Prox. Trap					
Max. sediment flux [g m^{-2} d^{-1}]	391	758	163	452	54
Sediment deposition [g m^{-2}]	1603	4320	2880	2825	1258
D : $Q_{prox.}$	No data	0·1	0·3	0·2	< 0·1
L : $U_{prox.}$	8	3	5	2	3
Dist. Trap					
Max. sediment flux [g m^{-2} d^{-1}]	No data	32	9	29	16
Sediment deposition [g m^{-2}]	No data	174	245	430	468
D : $Q_{dist.}$	No data	0·1	0·2	0·5	0·1
L : $U_{dist.}$	No data	1	2	1	3
PDI	No data	25	12	7	3

monitoring network (Table 1, Fig. 1). The June 2013 flood was exceptional for the entire observation period and reached by far the highest maximum discharge values (104 $m^3 s^{-1}$) and the longest duration (9 days >10 $m^3 s^{-1}$). The flood resulted in a lake level rise of more than 1·5 m and flooding of the city of Mondsee.

Suspended sediment concentration in the river (SSC), as recorded by turbidity measurements and automatic water samples, reached highest values during the 06/13 event (SSC_{max} = 61 g L^{-1} in samples, 103 g L^{-1} rated from turbidity) and was lowest during the 01/13 event (SSC_{max} = 1·1 g L^{-1} in samples, 1·6 g L^{-1} rated from turbidity). During all events, SSC increased with increasing discharge and reached maxima during the rising limb of the flood hydrograph and already declined 1 to 2 h before the flood peak (Figs 7 and 8).

The sediment depositions in the lake occurred with time lags of 1 to 4 days after the peak runoff at the proximal location and of up to 10 days at the distal trap (Figs 7 and 8). The total sediment deposition in the proximal basin was highest during the 06/12 event (4320 g m^{-2}) and lowest during the 07/13 event (1258 g m^{-2}), whereas at the distal site the opposite has been observed, i.e. highest sediment deposition during the 07/13 event (468 g m^{-2}) and lowest during the 06/12 event (174 g m^{-2}).

The sources of detrital sediment are determined by their mineralogical composition (Table 2). The sediments originating from the Flysch catchment predominately consist of siliciclastic material made up of quartz, mica and feldspars, whereas the Northern Calcareous Alps are predominantly composed of dolomite (Figure S1). This allows us to use the dolomite/quartz ratio (D : Q) to distinguish between the two main sediment source areas (Table 2). Riverbed material of the main tributaries Griesler and Wangauer Ache exhibit similar D : Q ratios of 0·2. This value is in accordance with most values measured in sediment trap samples in the lake, ranging between 0·2 and 0·5, indicating these catchments as main sources for detrital sediments. The lowest D : Q values <0·2 are measured for the Fischbach bed load reflecting a clear dominance of Flysch sediments in this sub-catchment that exclusively drains a Flysch area (Figure S1). Similar values are measured in sediments trapped after the local 06/12 and 07/13 events. The highest D : Q values >1·0 were measured for the bed load of the Kienbach creek reflecting a dominance of material originating from the Northern Calcareous Alps. Sediments trapped in the distal trap after the 06/13 flood exhibit D : Q values between 0·5 and 1·0 pointing to sediment transport from both, the Flysch and the Limestone catchments.

Sediment trap samples of the five events with highest sediment yields were further analysed for their grain size distribution (Fig. 9). The resulting distributions exhibit unimodal (prox.: 4 samples, dist.: 2 samples) and bimodal patterns (prox.: 1 samples, dist.: 4 samples) with maxima around 10 to 60 μm for unimodal and at 2 to 4 μm and 10 to 60 μm for bimodal functions, respectively. Thus, samples with a bimodal grain size distribution contain a higher portion of fine silt and clay particles. Fine-grained particles were generally more abundant in samples trapped (i) in summer, (ii) after the main sediment flux event and (iii) in the distal lake basin. The only exception is the June 2013 flood event (Fig. 9C), when trapped samples in the distal lake basin exhibited a unimodal function and a coarser maximum (36 μm) than in the proximal lake basin (24 μm).

DISCUSSION

Detrital layers in lake sediments commonly are interpreted as flood recorders. However, the potential of these geoarchives for extending instrumental flood records back in time is still not fully exploited due to our limited knowledge about (i) how the amount and spatial distribution of detrital sediment are related to flood parameters and (ii) to which extent this relation is affected by local factors in the catchment and the lake. These are considered as potential bias for establishing palaeoflood time series from lake sediment records (e.g. Schiefer *et al.*, 2006, 2011; Dugan *et al.*, 2009).

The 3-year monitoring at Lake Mondsee provides a comprehensive set of hydro-sedimentary data from the lake and its catchment comprising 26 floods with very different magnitudes (return periods ranging from ≪1 year to 100 years), seasonal occurrence and sediment response (4 to 758 g m^{-2} d^{-1}). This reveals new insights into processes of flood layer deposition with unprecedented detail including a variety of influencing factors like peak runoff and season, sediment availability or the type of precipitation event giving the basis for an improved evaluation of the depositional record of Lake Mondsee. Our monitoring data have been related to the available sub-recent depositional record covering the time period from 1976 to 2005 (Fig. 11) (Kämpf *et al.*, 2014) since it was not yet possible to obtain undisturbed sediment cores of the last 3 years due to the too high water content of the topmost sediments.

Parameters controlling flood-related sediment flux

Runoff magnitude

A general link between runoff events in the Griesler Ache and sediment flux into the lake is evidenced by the measured sediment response to 26 flood events. Moreover, we

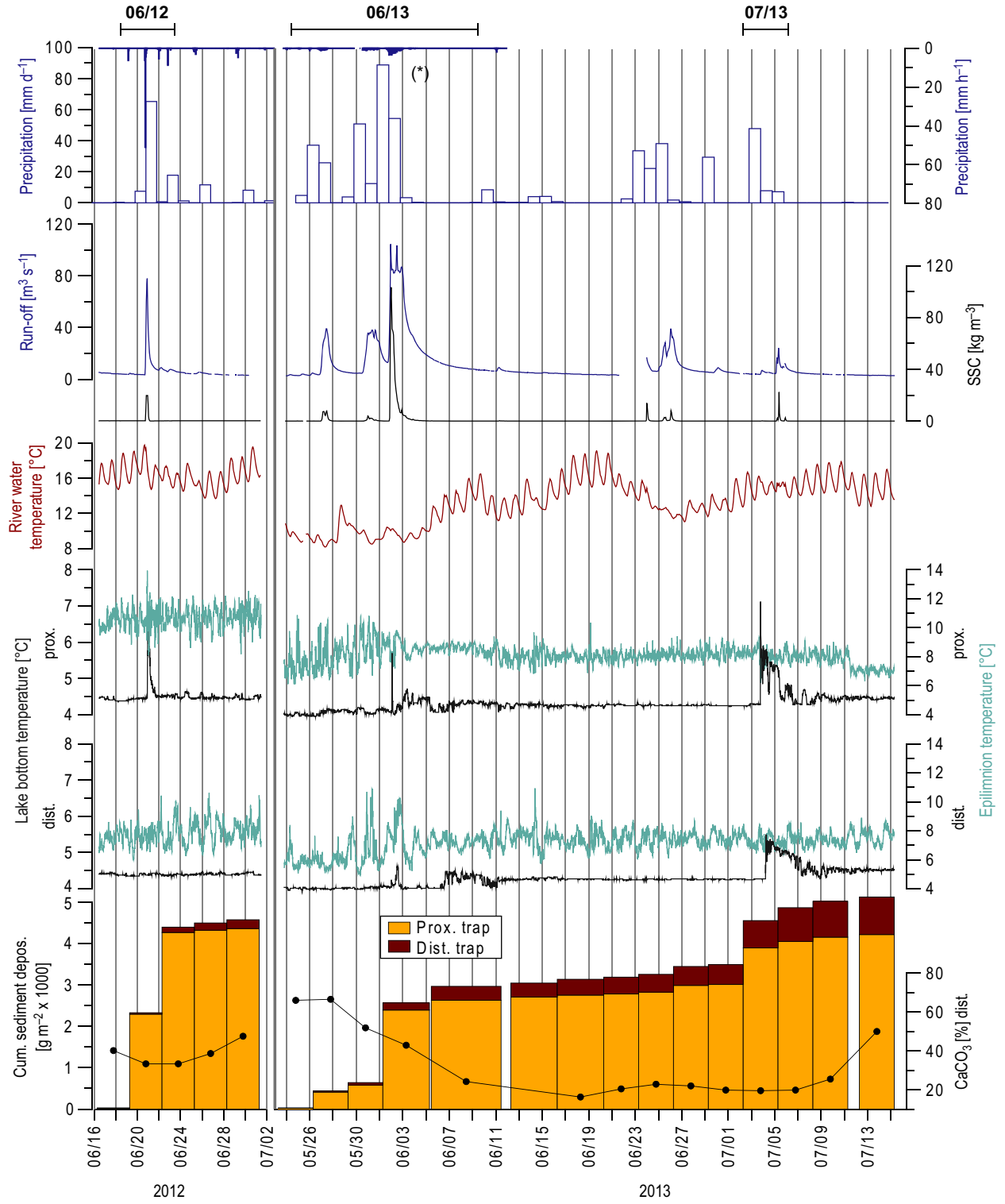

Fig. 7. Precipitation, runoff, river sediment concentration, river and lake water temperature and trapped sediment deposition 3 m above the lake bottom at the proximal and distal trap location during the largest summer floods. (*) Daily precipitation data from 2013 measured at the Oberwang gauging station. The distance between vertical grey lines represents 2 days.

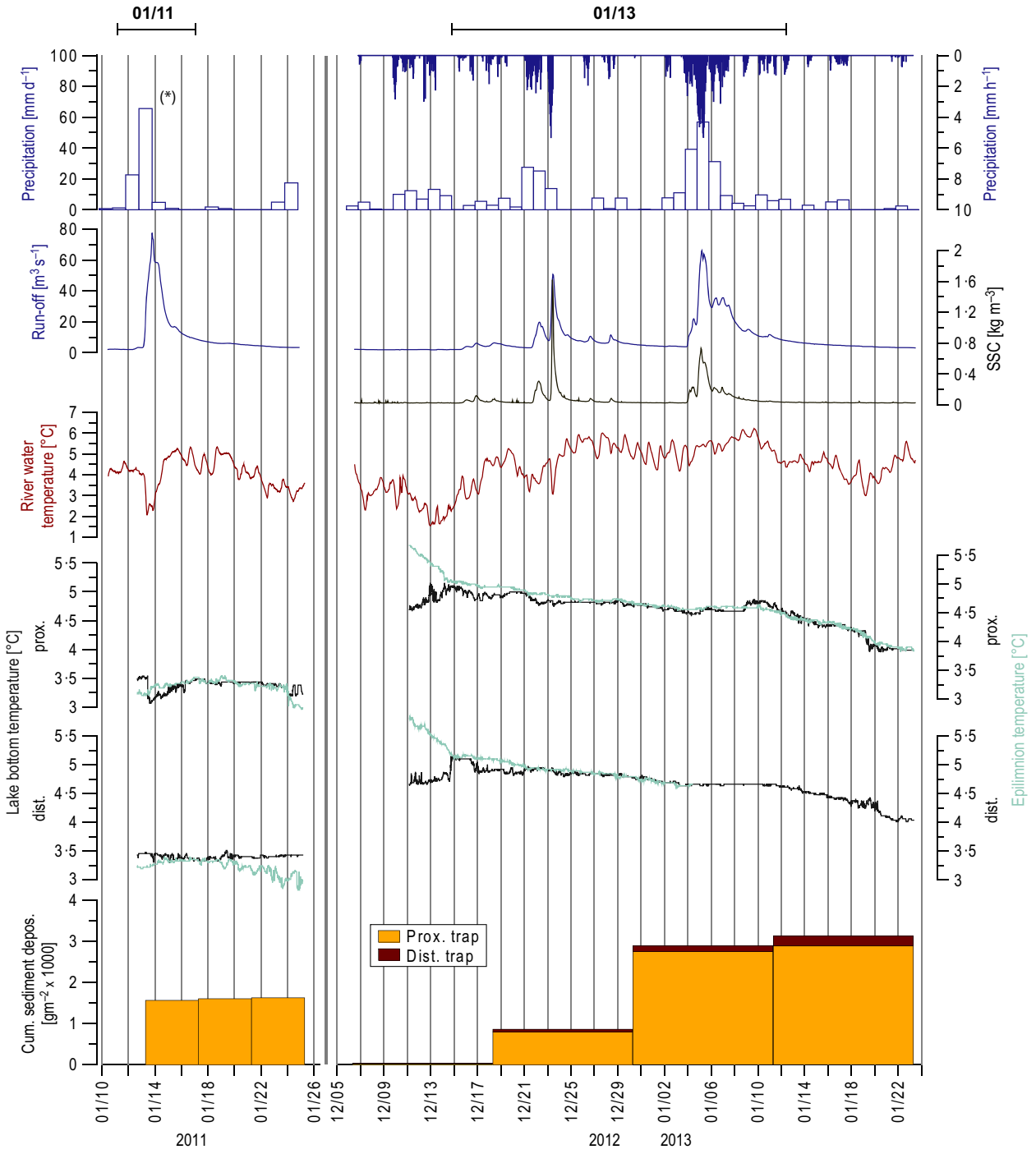

Fig. 8. Precipitation, run-off, river sediment concentration, river and lake water temperature and trapped sediment deposition 3 m above the lake bottom at the proximal and distal trap location during the largest winter floods. (*) Precipitation data from the 01/11 event measured at Thalgauberg gauging station. The distance between vertical grey lines represents 2 days.

found different empiric runoff thresholds for both sites, above which suspended sediment is transported to the respective location: 20 $m^3\ s^{-1}$ for the proximal and 30 $m^3\ s^{-1}$ for the distal site (Fig. 4). Lower amplitude floods caused a measurable sediment flux only in two exceptional cases.

In addition to the coincidence of peaks in the runoff and sediment trap time series, we observed a significant

Table 2. Mineralogical composition [%] of sediment trap samples obtained during major flood events (I = integral trap), river bed material and two detrital layers in the sub-recent sediment record. The ratio of dolomite and quartz contents (D : Q) was used to discriminate the Flysch (quartz-rich) and limestone (dolomite-rich) dominated sub-catchments (see also Figure S1).

Sample	Calcite	Chlorite	Dolomite	Kaolinite	Illite	Orthoclase	Albite	Quartz	Smectite	D : Q
Sediment traps										
13/6 prox.	26	4	6	2	10	3	4	28	16	0·2
13/6 prox._I_upper	32	4	5		9	2	3	27	18	0·2
13/6 prox._I_lower	27	4	6		10	3	5	29	17	0·2
13/7 prox.	25	5	2	4	12	3	4	31	15	0·1
13/1 prox.	25	3	9	2	7	3	7	35	10	0·3
12/6 prox.	21	5	4	3	11	3	5	31	17	0·1
13/6 dist.	43	4	18		10	2	2	20		0·9
13/6 dist._I_upper	41	3	4		9	2	2	20	20	0·2
13/6 dist._I_lower	38	4	9	3	8	2	2	19	15	0·5
13/7 dist.	23	5	2	3	12	2	2	26	25	0·1
13/1 dist.	33	4	6	3	10	2	3	24	16	0·2
12/6 dist.	35	4	2	4	12	3	2	22	18	0·1
River bed										
Griesler Ache	32		11			5	5	48		0·2
Kienbach	8		90					2		37·6
Wangauer Ache	57		6				3	33		0·2
Fischbach	19		4			6	7	64		0·1
Detrital layers										
DL 1986 dist.	18	3	64		2			8	5	7·7
DL 2002 prox.	21	5	2	4	13	3	4	28	20	0·1

exponential relation between peak runoff and the amount of trapped sediment in the proximal (r^2 = 0·76) and distal lake basin (r^2 = 0·80) if the local 07/13 event with predominant sediment flux from the ungauged secondary stream Wangauer Ache is excluded (Fig. 6A).

Hitherto, we only discussed the relation between runoff and sediment transport. More important for interpreting the depositional record, however, is an assessment of the amount of sediment flux that is necessary to produce a recognizable detrital layer in the sediment record. We can calculate this minimum sediment yield from the thickness of the finest detected detrital layers found in the sediments (0·2 mm; Kämpf *et al.*, 2014) and a mean dry density of 1·5 g cm^{-3}. The resulting minimum sediment yield of approximately 300 g m^{-2} was exceeded by four of the 26 observed floods at the proximal site that were triggered by runoff peaks ranging from 66 to 104 m^3 s^{-1} and precipitation >65 mm d^{-1} (Fig. 4, Table 1). At the distal site, where the long flood record has been established (Swierczynski *et al.*, 2013), only the strongest of these four events likely resulted in sufficient sediment transport to form a detrital layer (June 2013, max. runoff: 104 m^3 s^{-1}). Hence, based on the amount of sediment deposition we predict the formation of one flood triggered detrital layer at the distal location (June 2013) and four layers at the proximal site (January 2011, June 2012, January, June 2013). Another event in July 2013 that also supplied sediment amounts >300 g m^{-2} to the proximal and distal locations (Fig. 7) is not included in the further discussion since this event was caused by local precipitation in the Wangauer Ache catchment, which is not part of our monitoring network (Fig. 1).

The flood discharge values, which according to the observational data should have caused detrital layer formation, are for both locations in the same range as empirical discharge thresholds for detrital layers revealed from the depositional record (Kämpf *et al.*, 2014). These are >60 m^3 s^{-1} for the proximal site (observation: 66 m^3 s^{-1}, 78 m^3 s^{-1}, 104 m^3 s^{-1}) and >80 m^3 s^{-1} for the distal site (observation: 104 m^3 s^{-1}). The good agreement between these independently obtained data further supports the existence of discharge thresholds for flood layer deposition and makes us confident that these thresholds can be reasonable well determined.

Despite the existence of thresholds in discharge for detrital layer formation we do not observe a correlation between runoff and sediment yield for the strongest floods (Fig. 6B). This suggests that the availability of fine-grained sediment in the rivers and variable sediment distribution within the lake basin also play a crucial role for detrital layer formation and will be discussed in the following.

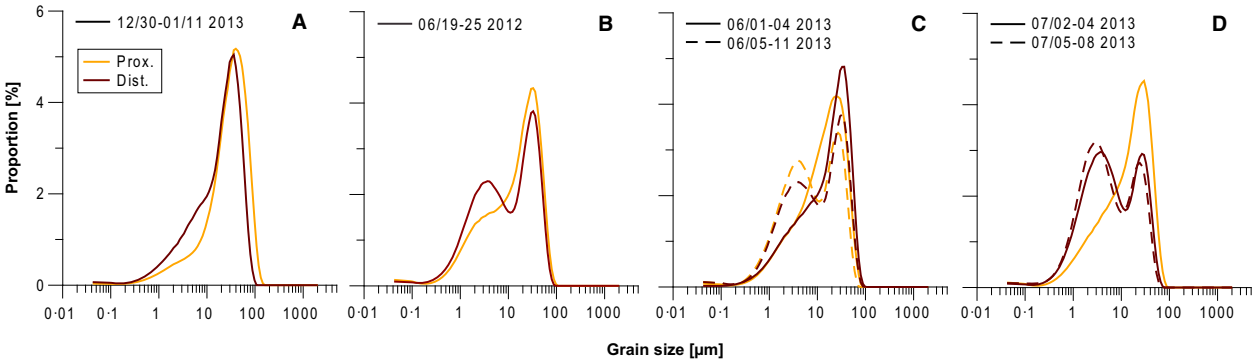

Fig. 9. Grain size distribution of trapped sediment samples of the four largest sediment transfer events: (A) 01/13, (B) 06/12, (C) 06/13, (D) 07/13. Straight-lined plots indicate sediment flux peak samples; dashed plots indicate samples after the sediment flux peaks.

Sediment availability

The measured variations in suspended sediment concentration in the streams provide evidence for the sediment availability in the catchment as an important factor (Fig. 10). Fine sediments are mainly derived from the channel bank of the streams but sometimes also from patches of local erosion events, e.g. landslides, as revealed by field observations after the 06/13 flood (Figure S3). The sediment input to the streams further depends on the season since measured sediment concentrations were much lower during the winter flood (01/13: max. 1 g L^{-1}) compared to summer floods (20 to 103 g L^{-1}). Although only two strong winter floods are observed, we assume that this seasonal difference is generally valid and can be explained by reduced soil erosion in winter due to snow cover and frozen ground (Dugan *et al.*, 2009).

Sediment availability is further changing within the course of a flood as demonstrated by the relation of river SSC and discharge (Fig. 10). Clockwise hysteresis functions indicate higher sediment concentrations during the rising limbs of the flood hydrographs proving river transport capacity as the main driver for riverine sediment transport in the initial phase of a flood when fine sediments are sufficiently available. In the later flood stage when sediments have been washed out and less fine material is available the riverine sediment transport is reduced as has been observed in various rivers (e.g. Forbes & Lamoureux, 2005; López-Tarazón *et al.*, 2010). This effect is also obvious from lower SSC values during the higher second flood peak of the 01/13 event which followed 13 days after a lower first runoff peak, which, in contrast, resulted in higher SSC values. For floods of only short duration, like the 06/12 event that lasted only for 18 hrs, river SSC followed the flood hydrograph during the rising and falling limb for the main flooding interval (>40 m^3 s^{-1}, 5 h) suggesting no limitations in sediment availability during such short floods.

Although the interpretation of the hysteresis plot of the strongest event (06/13) is limited because runoff during peak flow conditions (>100 m^3 s^{-1}) was likely underestimated due to river bank overflow, this example demonstrates that extreme high SSC values (>100 g L^{-1}) not necessarily result in the highest suspended sediment transport into the lake. If a certain threshold is reached and the floodplain becomes flooded, the flow velocity decreases and suspended sediment accumulates in the floodplain (Figure S3). This process is known as catchment storage (e.g. Orwin *et al.*, 2010) and is observed for the very strong 06/13 flood which led to lower amounts of trapped sediments than, for example, the 06/12 flood with much lower SSC values (max. 20 g L^{-1}).

Contrary with factors reducing sediment input to the lake, we also found few cases when sediment deposition can be significantly increased by additional sediment releases from local sources. Evidence for mixing of flood-triggered sediments from different sources is revealed for the distal location which is located ca. 800 m in front of the secondary Kienbach creek inflow (Fig. 1). The development of an underflow originating from the Kienbach and its impact on sediment deposition at the distal site can be demonstrated for the June 2013 flood. Besides tracing slumps in the head-catchment and the deposition of an approximately 0·5 m thick sediment fan of sand and gravel in the delta area of the Kienbach creek (Figure S3), we measured a 0·2 K temperature increase at the lake bottom at the distal site even 1 h before the temperature rise of the deep water at the proximal site (Fig. 7). This underflow did not reach the proximal site and thus reflects a local event with short travel time reaching the distal site before the underflow triggered by the main tributary (Griesler Ache). The Kienbach creek as sediment source is confirmed by coarser grain sizes (Fig. 9) and predominant dolomitic composition of the trapped sediments (Table 2) which reflects the Kienbach catchment geology of the Northern Calcareous Alps. In the

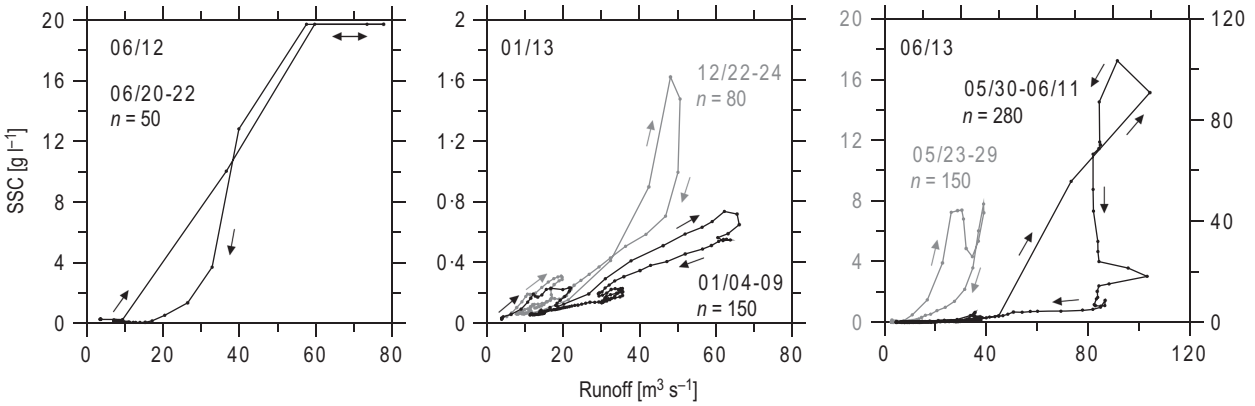

Fig. 10. River runoff – suspended sediment concentration (SSC) hysteresis plots for the three strongest recorded flood events in the Griesler Ache river (06/12, 01/13, 06/13). Note the different scaling of the y-axes. Dots mark single measurements in 1-hr intervals.

depositional record, local sediment flux from the Kienbach sub-catchment to the distal location has been suggested for four flood layers and for one debris flow layer (DL 16 in Fig. 11) deposited between 1976 and 2005 (Swierczynski *et al.*, 2009; Kämpf *et al.*, 2014).

In summary, the occurrence and thickness of detrital layers depends also on timing and preconditions of floods that might led to either an over- or an underestimation of the number of palaeofloods in the depositional record. On the one hand, detrital layers can be disproportionally thin or even miss when a flood followed a previous flood after a short time not sufficient to refill the riverbed with sediment or when catchment erosion is reduced (Czymzik *et al.*, 2010; Kämpf *et al.*, 2012b). On the other hand, additional sediment release from local sediment sources can result in the formation of non-flood triggered detrital layers or increase flood layer thickness (Girardclos *et al.*, 2007; Dugan *et al.*, 2009; Swierczynski *et al.*, 2009; Czymzik *et al.*, 2010). However, the potential bias by such local layers can be reduced by detailed micro-facies and geochemical analyses of individual detrital layers (Mangili *et al.*, 2005; Swierczynski *et al.*, 2009) and tracing detrital layers in multiple sediment cores (Lamoureux, 1999; Schiefer *et al.*, 2006, 2011; Kämpf *et al.*, 2012b, 2014).

Lake internal sediment distribution

The different spatial sediment distribution in the lake basin of individual events (PDI = 2 to 25) is related to variations in the formation of hyperpycnal underflows and mesopycnal interflows (Sturm & Matter, 1978; Chapron *et al.*, 2005). Sudden temperature increases of 2 to 3·5 K recorded in the deep water column during the largest summer floods proved the occurrence of underflows (Fig. 7). In winter, temperature fluctuations were less distinct or even negative (−0·4 K to +0·1 K in Fig. 8) due to the lower river water temperature. Underflows developed during the four strongest floods, but reached the distal site only during the 06/13 event 7 h after passing the proximal site. From this time lag, a minimum current speed of 9 cm s^{-1} can be calculated which is rather low compared to larger lakes where much stronger underflows were measured like, for example, lakes Walensee (20 to 50 cm s^{-1}), Geneva (30 to 90 cm s^{-1}) and Constance (30 to 130 cm s^{-1}) (Lambert *et al.*, 1976; Lambert & Giovanoli, 1988). The resulting lower sediment transport capacity of underflows in Lake Mondsee is proven also by the measured vertical differences in sediment flux in the proximal ($L : U_{prox.}$ = 2 to 8) and distal locations ($L : U_{dist.}$ = 1 to 2) indicating underflows as the predominant transport mechanism in the proximal and interflows in the distal lake basin.

The rather low number of underflows reaching the distal site compared to observations from other lakes (Schiefer *et al.*, 2006; Cockburn & Lamoureux, 2008; Jenny *et al.*, 2014) can be explained by the specific basin morphometry of Lake Mondsee (Fig. 1). At the point where the main tributary, the Griesler Ache, enters the lake, the elongated shape of the basin turns from NW-SE to N-S direction and later back to the original NW-SE direction. Due to this pronounced kink, the inflowing waters from the Griesler Ache are not straightaway directed towards the outflow but deflected first to the South and then to the East. Consequently, the flow velocity is expected to decrease, resulting in a lower sediment transport capacity. Lakes with frequent occurrence of underflows commonly have one large tributary stream and a simple elongated basin shape with straight flow direction from the main tributary inflow towards the outflow (Lambert *et al.*, 1976; Best *et al.*, 2005; Crookshanks & Gilbert, 2008; Jenny *et al.*, 2014).

The observed processes of detrital sediment distribution within Lake Mondsee provide explanations for the

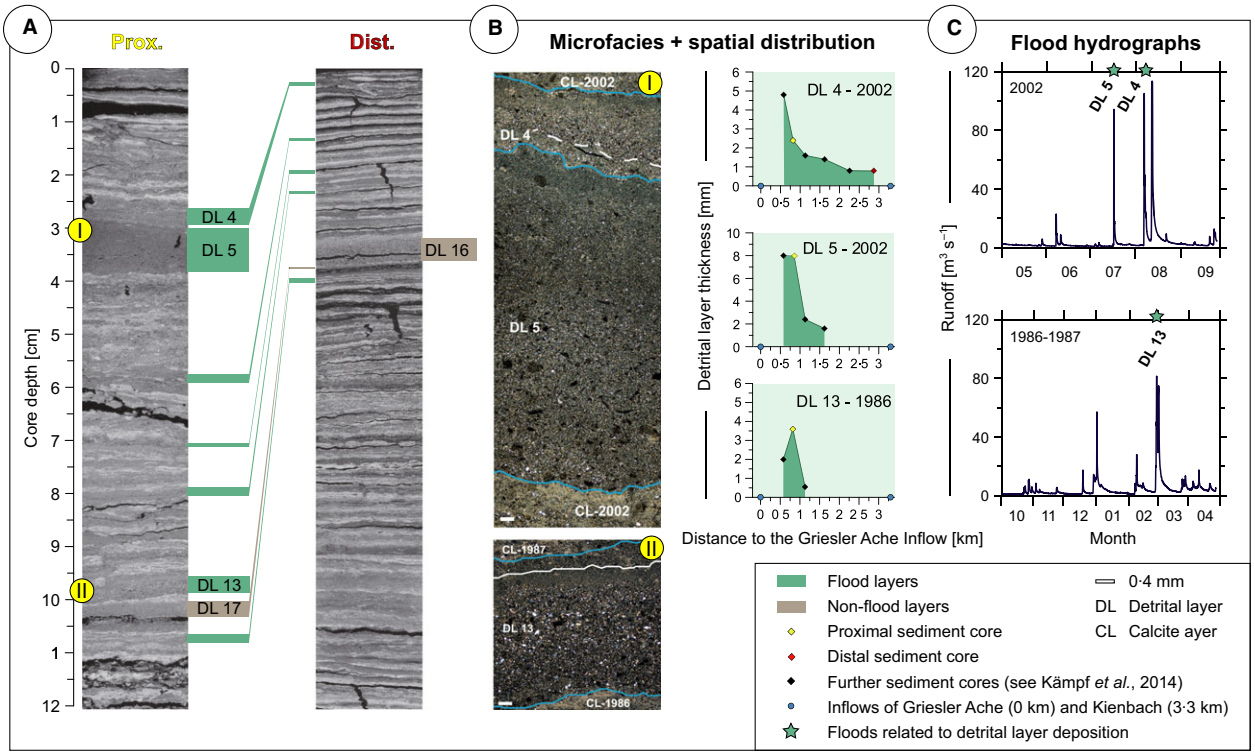

Fig. 11. Detrital layers in the varved sediment record of Lake Mondsee: (A) Thin section scans (polarized light) of the upper 12 cm of sediment cores close to the proximal and distal trap location (Fig. 1) and correlation of detrital layers, (B) microfacies of selected detrital layers (microscopic images under polarized light, 20× magnification) showing graded layers in the proximal core and different spatial distribution patterns, (C) seasonal flood hydrographs (hourly values) of the Griesler Ache River coincided to detrital layer deposition according to the seasonal resolution of the varved detrital layer record: summer = May-Sep and winter = Oct-Apr.

occurrence or absence of detrital layers in the depositional record obtained at the distal location (Swierczynski *et al.*, 2013). There, flood layers are mainly transported by interflows and appear as very fine, only microscopically detectable (0·2 to 0·8 mm), non-graded silt/clay layers, whereas graded layers triggered by underflows only occur at the proximal site in an area within 1·5 km around the river mouths (Fig. 11). Importantly, interflows are favoured in the summer season when the water column is stratified and a pycnocline develops along which sediment is transported. In contrast, even high amplitude winter floods supplied only small sediment amounts to the distal lake basin like the January 2013 flood; the sediment deposition (245 g m^{-2}) most likely was not sufficient to form a discernible detrital layer. This explains why the flood record from the distal site has been regarded as summer time series (Swierczynski *et al.*, 2012). To obtain a flood record including both summer and winter floods a coring site at the proximal position should be selected.

Another factor controlling the spatial distribution of detrital sediment within the lake basin is the flood duration. This can be demonstrated for sediment deposition during the short 06/12 event (74 mm rainfall in 4 h, Table 1) with a focal area at the proximal location since the under- and interflows broke down quickly when river discharge dropped and thus did not reach the distal basin as reflected by low sedimentation rates in the distal trap (Fig. 7). In contrast, the 06/13 flood lasted for 9 days resulting in strong and long lasting interflows as reflected by elevated sediment deposition at the distal trap over 10 days (Fig. 7).

Reconstructing palaeoflood time series in particular from distal sediment records, therefore, needs to concern not only about peak discharges but also the duration of floods. Strong but short floods might not reach the distal location but result in thick detrital layers in proximal cores (e.g. DL 5 in Fig. 11; associated peak runoff: 100 m^3 s^{-1}, daily mean: 24 m^3 s^{-1}). For the depositional record this means that (i) daily instead of hourly runoff values are more appropriate for defining discharge thresholds for detrital layer formation and (ii) distal coring locations are especially suitable for reconstructing large-scale rather than local flood events.

Implications for the use of detrital layers as flood proxies

Our monitoring data provide clues for both, (i) reliable interpretation of detrital layers as flood proxies and (ii) selecting suitable coring locations for palaeoflood reconstruction.

The monitoring data reveals that thresholds in discharge exist, above which flood layer formation becomes very likely. Obviously, these thresholds depend on the coring location and most likely vary also for different lakes (Czymzik *et al.*, 2010; Kämpf *et al.*, 2012b; Corella *et al.*, 2014; Jenny *et al.*, 2014). However, the monitoring and its comparison with the sediment record demonstrate that these thresholds can be empirically determined and thus provide information about the minimum amplitude of floods recorded in depositional records.

Reconstructing individual flood amplitudes from detrital layer thickness, however, still remains challenging. For Lake Mondsee with a complex lake basin morphometry, a vegetated catchment and sediments predominantly produced in the water column through biological productivity, this approach failed because several other factors including sediment availability, local sediment supply and lake internal sediment distribution significantly bias magnitude estimates of palaeofloods. In contrast, for small proglacial and nival lakes with one main tributary inflow and predominantly clastic-detrital sedimentation a correlation between peak runoff and sediment flux has been demonstrated (Desloges & Gilbert, 1994; Chutko & Lamoureux, 2008; Schiefer *et al.*, 2011). More lakes must be investigated to find out if there is a systematic difference between lakes with different settings and sediment types.

Detrital layer successions in depositional records should not per se be considered as complete flood time series. We have demonstrated that there might be additional layers due to local sediment transport but also 'missing' layers, i.e. floods that did not result in detrital layer formation. This can be either due to random or systematic processes, like the lack of winter flood layers at the distal location in Lake Mondsee. Both, additional, non-flood triggered, and missing layers represent a potential and assumedly site specific bias in flood reconstruction. However, we have also demonstrated that it is possible to reduce the potential bias through (i) detailed micro-facies and geochemical analyses and (ii) a careful choice of coring sites ideally integrating proximal and distal locations (Czymzik *et al.*, 2010; Schiefer *et al.*, 2011; Jenny *et al.*, 2014; Kämpf *et al.*, 2014).

Although flood reconstructions are conducted to a wide range of lakes, varved sediment records provide particularly suitable archives for process studies to develop quantitative flood proxies in terms of their hydrological characteristics.

CONCLUSIONS

The 3-year integrated lake and catchment flood monitoring at Lake Mondsee revealed detailed insights into the complex chain of processes leading to flood layer formation. In particular, reasons for variable sediment flux at the lake floor could be identified including hydrological factors such as runoff magnitude and duration, local geomorphological factors influencing sediment availability in the catchment and factors controlling the spatial distribution of detrital material within the lake. This knowledge has implications for the long flood record established at the distal lake basin of Lake Mondsee:

1 Threshold processes in the runoff – sediment flux relation define flood magnitudes above which suspended matter is transported and detrital layers are formed. The long Lake Mondsee flood layer chronology records all floods exceeding 80 $m^3 s^{-1}$ river discharge and lasting for at least 2 days.
2 The depositional record at the distal site represents mainly summer floods due to the seasonally favoured development of mesopycnal interflows, the main transport agent for lake internal sediment distribution. Winter flood layers, deposited by hyperpycnal underflows, can be only found at core locations close to the river inflow.
3 Reconstruction of flood amplitudes by layer thickness is limited because the sediment yield after floods is not linearly related to runoff but is additionally affected by various other geomorphological and lake internal factors.
4 The potential bias of detrital layers triggered by local erosion events rather than by high magnitude floods can be reduced by detailed micro-facies and high-resolution geochemical analyses.

It has been shown that comparison of sediment monitoring with sub-recent detrital layer records provides valuable information for an advanced interpretation of detrital layers as flood recorders and for systematic selection of the most suitable coring location within a lake basin. Even if our dataset obviously is to a certain degree site specific for Lake Mondsee, we expect the fundamental mechanisms and controlling processes as valid also for many other lake sites.

ACKNOWLEDGEMENTS

This study contributes to the Potsdam Research Cluster for Georisk Analysis, Environmental Change and Sustainability (PROGRESS) part A.3 'Extreme events in geoarchives'

funded by the German Federal Ministry for Education and Research (BMBF). We are especially grateful to Prof. Rainer Kurmayer and Prof. Thomas Weisse (both University of Innsbruck, Research Institute for Limnology Mondsee) for their support and scientific collaboration as well as to Kurt Mayrhofer (University of Innsbruck, Research Institute for Limnology Mondsee), Richard Niederreiter (UWITEC) and numerous students for technical support and help during field work. We further thank Sebastian Lorenz (University of Greifswald) for his help during grain size measurements, Petra Meyer (GFZ Potsdam) for elemental analyses as well as Georg Schettler and Jens Mingram (both GFZ Potsdam) for useful advices regarding the monitoring set-up and lab analyses. Andreas Hendrich (GFZ Potsdam) is acknowledged for his help with illustrating the figures. We thank two anonymous reviewers for constructive comments which helped to improve the manuscript.

References

Arnaud, F., Revel, M., Chapron, E., Desmet, M. and Tribovillard, N. (2005) 7200 years of Rhône river flooding activity in Lake Le Bourget, France: a high-resolution sediment record of NW Alps hydrology. Holocene, **15**, 420–428.

Best, J.L., Kostaschuk, R.A., Peakall, J., Villard, P.V. and Franklin, M. (2005) Whole flow field dynamics and velocity pulsing within natural sediment-laden underflows. Geology, **33**, 765.

Blöschl, G., Nester, T., Komma, J., Parajka, J. and Perdigão, R.A.P. (2013) The June 2013 flood in the Upper Danube basin, and comparisons with the 2002, 1954 and 1899 floods. Hydrol. Earth Syst. Sci., **17**, 5197–5212.

BMLFUW (2011) Hydrographisches Jahrbuch von Österreich 2011. BMLFUW, Vienna, 967 pp.

Chapron, E., Arnaud, F., Noël, H., Revel, M., Desmet, M. and Perdereau, L. (2005) Rhone River flood deposits in Lake Le Bourget: a proxy for Holocene environmental changes in the NW Alps, France. Boreas, **34**, 404–416.

Chutko, K.J. and Lamoureux, S.F. (2008) Identification of coherent links between interannual sedimentary structures and daily meteorological observations in Arctic proglacial lacustrine varves: potentials and limitations. Can. J. Earth Sci., **45**, 1–13.

Cockburn, J.M.H. and Lamoureux, S.F. (2008) Inflow and lake controls on short-term mass accumulation and sedimentary particle size in a High Arctic lake: implications for interpreting varved lacustrine sedimentary records. J. Paleolimnol., **40**, 923–942.

Corella, J.P., Benito, G., Rodriguez-Lloveras, X., Brauer, A. and Valero-Garcés, B.L. (2014) Annually-resolved lake record of extreme hydro-meteorological events since AD 1347 in NE Iberian Peninsula. Quatern. Sci. Rev., **93**, 77–90.

Crookshanks, S. and Gilbert, R. (2008) Continuous, diurnally fluctuating turbidity currents in Kluane Lake, Yukon Territory. Can. J. Earth Sci., **45**, 1123–1138.

Czymzik, M., Dulski, P., Plessen, B., von Grafenstein, U., Naumann, R. and Brauer, A. (2010) A 450 year record of spring-summer flood layers in annually laminated sediments from Lake Ammersee (southern Germany). Water Resour. Res., **46**, W11528.

Czymzik, M., Brauer, A., Dulski, P., Plessen, B., Naumann, R., von Grafenstein, U. and Scheffler, R. (2013) Orbital and solar forcing of shifts in Mid- to Late Holocene flood intensity from varved sediments of pre-alpine Lake Ammersee (southern Germany). Quatern. Sci. Rev., **61**, 96–110.

Desloges, J.R. and Gilbert, R. (1994) Sediment source and hydroclimatic inferences from glacial lake sediments: the postglacial sedimentary record of Lillooet Lake, British Columbia. J. Hydrol., **159**, 375–393.

Dokulil, M. and Skolaut, C. (1986) Succession of phytoplankton in a deep stratifying lake: Mondsee, Austria. Hydrobiologica, **138**, 9–24.

Dugan, H.A., Lamoureux, S.F., Lafrenière, M.J. and Lewis, T. (2009) Hydrological and sediment yield response to summer rainfall in a small high Arctic watershed. Hydrol. Process., **23**, 1514–1526.

Eybl, J., Godina, R., Lalk, P., Lorenz, P., Müller, G., Pavlik, H., Weilguni, V. and Heilig, M. (2013) Hochwasser im Juni 2013 – Die hydrographische Analyse. BMLFUW, Vienna, Austria.

Forbes, A. and Lamoureux, S. (2005) Climatic controls on streamflow and suspended sediment transport in three large Middle Arctic Catchments, Boothia Peninsula, Nunavut, Canada. Arct. Antarct. Alpine Res., **37**, 304–315.

Francus, P., Bradley, R.S., Abbott, M.B., Patridge, W. and Keimig, F. (2002) Paleoclimate studies of minerogenic sediments using annually resolved textural parameters. Geophys. Res. Lett., **29**, 1998.

Gilbert, R., Crookshanks, S., Hodder, K.R., Spagnol, J. and Stull, R.B. (2006) The record of an extreme flood in the sediments of Montane Lillooet Lake, British Columbia: implications for paleoenvironmental assessment. J. Paleolimnol., **35**, 737–745.

Girardclos, S., Schmidt, O.T., Sturm, M., Ariztegui, D., Pugin, A. and Anselmetti, F.S. (2007) The 1996 AD delta collapse and large turbidite in Lake Brienz. Mar. Geol., **241**, 137–154.

Glur, L., Wirth, S.B., Büntgen, U., Gilli, A., Haug, G.H., Schär, C., Beer, J. and Anselmetti, F.S. (2013) Frequent floods in the European Alps coincide with cooler periods of the past 2500 years. Sci. Rep., **3**, 2770.

Hsü, K.J. and Kelts, K. (1985) Swiss lakes as a geological laboratory. Naturwissenschaften, **72**, 315–321.

Jenny, J.-P., Wilhelm, B., Arnaud, F., Sabatier, P., Giguet Covex, C., Mélo, A., Fanget, B., Malet, E., Ployon, E. and

Perga, M.E. (2014) A 4D sedimentological approach to reconstructing the flood frequency and intensity of the Rhône River (Lake Bourget, NW European Alps). J. Paleolimnol., **51**, 469–483.

Kämpf, L., Brauer, A., Dulski, P., Feger, K., Jacob, F. and Klemt, E. (2012a) Sediment imprint of the severe 2002 summer flood in the Lehnmühle reservoir, eastern Erzgebirge (Germany). E&G Quatern. Sci. J., **61**, 3–15.

Kämpf, L., Brauer, A., Dulski, P., Lami, A., Marchetto, A., Gerli, S., Ambrosetti, W. and Guilizzoni, P. (2012b) Detrital layers marking flood events in recent sediments of Lago Maggiore (N. Italy) and their comparison with instrumental data. Freshwat. Biol., **57**, 2076–2090.

Kämpf, L., Brauer, A., Swierczynski, T., Czymzik, M., Mueller, P. and Dulski, P. (2014) Processes of flood-triggered detrital layer deposition in the varved Lake Mondsee sediment record revealed by a dual calibration approach. J. Quatern. Sci., **29**, 475–486.

Koschel, R., Brenndorf, J., Proft, G. and Recknagel, R. (1983) Calcite precipitation as a natural mechanism of eutrophication. Arch. Hydrobiol., **98**, 380–408.

Lambert, A. and Giovanoli, F. (1988) Records of riverbome turbidity currents and indications of slope failures in the Rhone delta of Lake Geneva. Limnol. Oceanogr., **33**, 458–468.

Lambert, A., Kelts, K. and Marshall, N.F. (1976) Measurements of density underflows from Walensee, Switzerland. Sedimentology, **23**, 87–105.

Lamoureux, S. (1999) Spatial and interannual variations in sedimentation patterns recorded in nonglacial varved sediments from the Canadian High Arctic. J. Paleolimnol., **21**, 73–84.

Lamoureux, S.F., Stewart, K.A., Forbes, A.C. and Fortin, D. (2006) Multidecadal variations and decline in spring discharge in the Canadian middle Arctic since 1550 AD. Geophys. Res. Lett., **33**, L02403.

Lapointe, F., Francus, P., Lamoureux, S.F., Saïd, M. and Cuven, S. (2012) 1750 years of large rainfall events inferred from particle size at East Lake, Cape Bounty, Melville Island, Canada. J. Paleolimnol., **48**, 159–173.

Lauterbach, S., Brauer, A., Andersen, N., Danielopol, D.L., Dulski, P., Hűls, M., Milecka, K., Namiotko, T., Obremska, M., von Grafenstein, U. and Participants, D. (2011) Environmental responses to Lateglacial climatic fluctuations recorded in the sediments of pre-Alpine Lake Mondsee (northeastern Alps). J. Quatern. Sci., **26**, 253–267.

Lewis, J. (1996) Turbidity-controlled suspended sediment sampling for runoff-event load estimation. Water Resour. Res., **32**, 2299–2310.

Lewis, J. and Eads, R. (2009) Implementation Guide for Turbidity Threshold Sampling: Principles, Procedures, and Analysis. USDA.

López-Tarazón, J.A., Batalla, R.J., Vericat, D. and Balasch, J.C. (2010) Rainfall, runoff and sediment transport relations in a mesoscale mountainous catchment: The River Isábena (Ebro basin). Catena, **82**, 23–34.

Mangili, C., Brauer, A., Moscariello, A. and Naumann, R. (2005) Microfacies of detrital event layers deposited in Quaternary varved lake sediments of the Pianico-Sellere Basin (northern Italy). Sedimentology, **52**, 927–943.

Meyers, P.A. and Teranes, J.L. (2001) Sediment organic matter. In: Tracking Environmental Change Using Lake Sediments. Volume 2: Physical and Geochemical Methods (Eds W.M. Last and J.P. Smol), pp. 239–269. Kluwer Academic Publishers, Dordrecht, The Netherlands.

Mueller, P., Thoss, H., Kaempf, L. and Güntner, A. (2013) A buoy for continuous monitoring of suspended sediment dynamics. Sensors, **13**, 13779–13801.

Orwin, J.F., Lamoureux, S.F., Warburton, J. and Beylich, A. (2010) A framework for characterizing fluvial sediment fluxes from source to sink in cold environments. Geogr. Ann., **92**, 155–176.

Schiefer, E., Menounos, B. and Slaymaker, O. (2006) Extreme sediment delivery events recorded in the contemporary sediment record of a montane lake, southern Coast Mountains, British Columbia. Can. J. Earth Sci., **43**, 1777–1790.

Schiefer, E., Gilbert, R. and Hassan, M.A. (2011) A lake sediment-based proxy of floods in the Rocky Mountain Front Ranges, Canada. J. Paleolimnol., **45**, 137–149.

Schlolaut, G., Brauer, A., Marshall, M.H., Nakagawa, T., Staff, R.A., Bronk Ramsey, C., Lamb, H.F., Bryant, C.L., Naumann, R., Dulski, P., Brock, F., Yokoyama, Y., Tada, R. and Haraguchi, T. (2014) Event layers in the Japanese Lake Suigetsu "SG06" sediment core: description, interpretation and climatic implications. Quatern. Sci. Rev., **83**, 157–170.

Siegenthaler, C. and Sturm, M. (1991) Die Häufigkeit von Ablagerungen extremer Reuss-Hochwasser : Die Sedimentationsgeschichte im Urnersee seit dem Mittelalter. Mitt. Bundesamt für Wasserwirtschaft, **4**, 127–139.

Støren, E.N., Dahl, S.O., Nesje, A. and Paasche, Ø. (2010) Identifying the sedimentary imprint of high-frequency Holocene river floods in lake sediments: development and application of a new method. Quatern. Sci. Rev., **29**, 3021–3033.

Sturm, M. and Matter, A. (1978) Turbidites and varves in Lake Brienz (Switzerland): deposition of clastic detritus by density currents. Int. Assoc. Sedimentol. Spec. Publ., **2**, 147–178.

Swierczynski, T., Lauterbach, S., Dulski, P. and Brauer, A. (2009) Die Sedimentablagerungen des Mondsees (Oberösterreich) als ein Archiv extremer Abflussereignisse der letzten 100 Jahre. In: Klimawandel in Österreich – Die letzten 20.000 Jahre. . .und ein Blick voraus (Eds R. Schmidt, C. Matulla and R. Psenner), pp. 115–126. Innsbruck University Press, Innsbruck, Austria.

Swierczynski, T., Brauer, A., Lauterbach, S., Martín-Puertas, C., Dulski, P., von Grafenstein, U. and Rohr, C. (2012)

A 1600 yr seasonally resolved record of decadal-scale flood variability from the Austrian Pre-Alps. Geology, **40**, 1047–1050.

Swierczynski, T., Lauterbach, S., Dulski, P., Delgado, J., Merz, B. and Brauer, A. (2013) Mid- to late Holocene flood frequency changes in the northeastern Alps as recorded in varved sediments of Lake Mondsee (Upper Austria). Quatern. Sci. Rev., **80**, 78–90.

Van Husen, D. (1989) Blatt 65–Mondsee. Geol. Karte der Republik Österreich 150 000

Wilhelm, B., Arnaud, F., Sabatier, P., Magand, O., Chapron, E., Courp, T., Tachikawa, K., Fanget, B., Malet, E., Pignol, C., Bard, E. and Delannoy, J.J. (2013) Palaeoflood activity and climate change over the last 1400 years recorded by lake sediments in the north-west European Alps. J. Quatern. Sci., **28**, 189–199.

Wirth, S.B., Gilli, A., Simonneau, A., Ariztegui, D., Vannière, B., Glur, L., Chapron, E., Magny, M. and Anselmetti, F.S. (2013a) A 2000 year long seasonal record of floods in the southern European Alps. Geophys. Res. Lett., **40**, 4025–4029.

Wirth, S.B., Glur, L., Gilli, A. and Anselmetti, F.S. (2013b) Holocene flood frequency across the Central Alps – solar forcing and evidence for variations in North Atlantic atmospheric circulation. Quatern. Sci. Rev., **80**, 112–128.

Supporting Information

Additional Supporting Information may be found in the online version of this article:

Figure S1. Mineralogical composition of river bed samples (blue arrow) and detrital layers in sediment cores (red arrow).

Figure S2. Calibration of turbidity of the Griesler Ache River recorded at St. Lorenz gauging station against suspended sediment concentration (SSC) derived from automatically taken water samples for the three flood events 06/12, 01/13 and 06/13.

Figure S3. Photographs documenting fluvial and in-lake sediment transport: (A) 06/13 event: channel bank erosion at Fischbach (SWB station), (B) 06/13 event: slump in the Kienbach valley, (C) 06/13 event: deposition of a ca. 0·5 m thick fan of sand and gravel in the Kienbach delta (A to C: photographs taken on 12 June 2013), (D) 01/11 event: Griesler Ache at St. Lorenz gauging station (14 January 2011 09:40 a.m.; runoff = 48 $m^3\ s^{-1}$), (E) 06/13 event: Griesler Ache close to St. Lorenz gauging station (02 June 2013 06:00 p.m.; runoff = 83 $m^3\ s^{-1}$, SSC = 7 g L^{-1}), (C) 06/12 event: Griesler Ache inflow into Lake Mondsee; (21 June 2012 12:10 p.m., runoff = 10 $m^3\ s^{-1}$, SSC = 0·1 g L^{-1}).

